Orbital Occupation in Electron-Charged CdSe Quantum-Dot Solids

Arjan J. Houtepen* and Daniël Vanmaekelbergh

Debye Institute, University Utrecht, POB 80000, 3508 TA Utrecht, The Netherlands

Received: June 9, 2005; In Final Form: August 19, 2005

We have prepared high-quality assemblies of monodisperse CdSe quantum dots and employed a combination of electrochemical gating and electrical and optical techniques to study orbital occupation in these quantum-dot solids. Electron occupation in localized states is important in some cases and can be unambiguously distinguished from occupation of the nanocrystal eigenstates. In addition, all excitonic transitions show a red-shift in the transition energy, due to the presence of electron charge. We infer that the energy of the S electrons is determined by the quantum-confinement energy and by Coulomb repulsions of the S electron with all other electrons in the assembly. By using a simple electron-repulsion model, we explain observed differences in the electron-addition energy for different samples, the broadening of the electron occupation as a function of electrochemical potential, and the strong dependence of the electron-addition energy on nanocrystal diameter.

Introduction

Assemblies of semiconductor nanocrystals, so-called quantum-dot solids, form an interesting class of new materials.[1] The optoelectronic properties of such systems can be tuned by choice of the semiconductor nanocrystals (the building blocks) and the electronic interactions between them.[2,3] The properties of the building blocks are determined by confinement of the electron or hole inside the nanocrystal host. Quantum confinement leads to a set of discrete conduction-electron and valence-hole orbitals (instead of bands) and a "band" gap that increases in energy with decreasing crystal size. For II−VI compound nanocrystals, the conduction states have S, P, D, and so forth symmetry and are well separated in energy (100 meV or more). The dipole and electronic coupling between the nanocrystals in the assembly depend on the distance between them, as well as the nature and length of the nanocrystal capping molecules and molecular linkers.[4]

A semiconductor quantum dot with one—or more—electrons in the S, P, and so forth conduction orbitals can be considered as an artificial atom. The intraband optical transitions, for example, obey the same selection rules as ordinary atoms (i.e., $\Delta l = \pm 1$).[5] Study of the electronic transport properties of electron-charged quantum-dot solids, determined by the orbital occupation, is of great fundamental interest. Electron-charged quantum-dot solids may become important in the optoelectronic industry, for example, for LEDs,[6−8] low-threshold lasers,[9] and solar cells. It has been shown that "electrochemical gating" provides a reversible and well-controlled method for charging quantum-dot solids with electrons.[10−12] The method is based on compensation of the electron charge by positive ions filling the voids of the quantum-dot assembly. Electrochemical electron injection into quantum-dot solids consisting of ZnO, PbSe, and CdSe nanocrystals has been reported.[5,12−15] Quantum-dot solids comprising colloidal CdSe nanocrystals form an important case for fundamental study. The electronic structure[16] and the optical properties[17,18] of CdSe have been studied in detail. This has led to an understanding of the fundamental and higher-energy excitonic transitions in terms of the nanocrystal eigenstates. Electrochemical electron injection in a CdSe quantum-dot solid has been studied previously by Yu et al.[12] By using a combination of electrochemical, electrical, and optical techniques, they showed that electrons occupy sequentially the S and P conduction orbitals and that occupation of these orbitals determines the electronic conductivity of the solids. In addition, the same group showed that electron-charged CdSe quantum-dot solids may be an important step forward in the development of low-threshold lasers.[9]

Here, we present a detailed study of electron-charged CdSe quantum-dot solids, consisting of nanocrystal building blocks between 3 and 9 nm in diameter. This work was motivated by a number of unanswered questions on the nature of the electron states, the influence of electronic occupation and electron charge on the fundamental and higher-energy exciton transitions, and the thermodynamic aspects of electron injection. Our preliminary measurements suggested that localized electron levels, that is, traps, could play a role in the charging characteristics and in the optical properties. We have employed a combination of electrochemical (differential capacitance), electrical (conductance), and optical techniques (absorption spectroscopy) to study orbital occupation under steady-state conditions. It will be shown that electron occupation in localized states is important in some cases and can be unambiguously distinguished from occupation of the nanocrystal eigenstates. Second, we show that all excitonic transitions show a red-shift in the transition energy, due to the presence of electron charge. Third, to investigate the factors which determine the energetics of electron charging, we monitored the electron occupation of the LUMO (S-type conduction orbital) by measurement of the absorption quenching as a function of the electrochemical potential. We show that the energy of the S electrons is determined by the quantum-confinement energy, and by Coulomb repulsions of the S electron with all other electrons in the assembly.

* Author to whom correspondence should be addressed. E-mail: a.j.houtepen@phys.uu.nl.

10.1021/jp053103i CCC: $30.25
Published on Web 10/01/2005

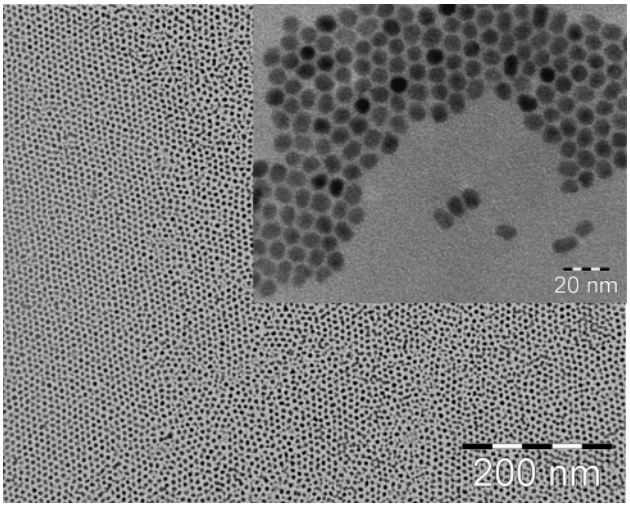

Figure 1. TEM image of 6.2 nm CdSe nanoparticles. The insert shows a magnified image of an 8.4 nm CdSe nanocrystal monolayer.

Experimental Section

Colloidal CdSe nanocrystals used for these experiments were prepared by high-temperature organometallic synthesis, as first described by Murray et al.[19] The exact conditions were those used by de Mello Donega et al.[20] The entire synthesis and subsequent steps are carried out in the inert atmosphere of an argon-purged glovebox. This procedure yields particles with an average diameter of 2.9 nm, a high luminescence quantum yield (40−80%), and a narrow size distribution (< 10% standard deviation). To obtain larger particles, appropriate amounts of $Cd(CH_3)_2$ and Se dissolved in trioctyl phosphate (TOP) are added dropwise to the solution with 2.9 nm particles at 240 °C. With this method, CdSe nanocrystals were synthesized ranging in diameter from 2.9 to 8.4 nm. The quantum-dot solution was cleaned by adding a small amount of anhydrous methanol, which caused the nanocrystals to precipitate. No size-selective precipitation techniques were applied to these samples. The capping layer of TOP−TOPO−HDA (TOPO = trioctylphosphine oxide; HDA = hexadecylamine) was replaced with pyridine by dispersing the nanocrystals in pure pyridine and heating this solution to 60 °C overnight. This was done to decrease the average distance between the CdSe nanocrystals in the assembly.[4,21] Figure 1 shows a monolayer of quantum dots of 6.2 and 8.4 nm (insert).

Quantum-dot solids were prepared by dropcasting a dispersion of CdSe nanocrystals in methanol/pyridine (1:1 v/v). The concentration of nanocrystals, determined via the optical density,[22] was roughly 2 μM. A few drops of this solution were dropped on a conducting substrate. The substrate was either an untreated ITO electrode or a gold electrode with a source and a drain, treated with 1,6-hexanedithiol. After the quantum-dot assembly had dried, it was treated with 1,6-heptanediamine, which serves to cross-link the nanoparticles. The presumed effect of this cross-linking procedure is to decrease the distance between the quantum dots; it leads to a much higher conductivity in these samples.[4,21,23] The electrode with the assembly was held in a 10 mM solution of the cross-linker in acetonitrile for 1 min. Subsequently, it was annealed at 70 °C for 1 h and placed under vacuum overnight to remove any residual traces of solvent. The thickness of the nanoparticle films, as determined by the optical density and profilometry (Tencor Instruments alphastep 500), ranged from 200 to 500 nm.

The electron occupation of the quantum-dot assemblies was controlled by "electrochemical gating".[24] The setup used for these experiments is described in detail elsewhere.[25] Briefly, the conducting substrate in electrical contact with the quantum-dot layer forms the working electrode (WE) in a three-electrode electrochemical cell. Platinum was used as the counter electrode (CE). The potential of the working electrode is controlled by a potentiostat (Princeton Applied Research Potentiostat/Galvanostat 273A) with respect to a Ag pseudo-reference electrode. When the WE potential is made more negative, electrons are injected into the assembly. Charge compensation is achieved by cations permeating the voids of the assembly. All experiments were performed in an airtight Teflon cell with quartz windows for optical measurements. The electrolyte solution was 0.1 M $LiClO_4$ in anhydrous acetonitrile. The silver pseudo-reference electrode was calibrated for each experiment with the ferrocene/ferrocinium couple, and the potential was converted to the normal hydrogen electrode (NHE) scale.[26] The cell was loaded inside an argon-purged glovebox to ensure water- and oxygen-free conditions. In conventional electrochemical techniques (such as cyclic voltammetry), slow dynamics might prevent the system from reaching electrochemical equilibrium. To ensure steady-state conditions, differential capacitance measurements were performed by applying a small (25mV) step in the potential of the working electrode and monitoring the current. The integrated current corrected for a Faradaic background current gives the charge that is introduced into the sample after the potential step. A comparison between the differential capacitance and the cyclic voltammogram of a CdSe assembly is presented in the Supporting Information. The injected charge is proportional to the differential capacitance at the electrochemical potential of the working electrode: $C(V) = \Delta Q/\Delta V$. This is a direct measure of the density of states of the CdSe quantum-dot assembly.[25]

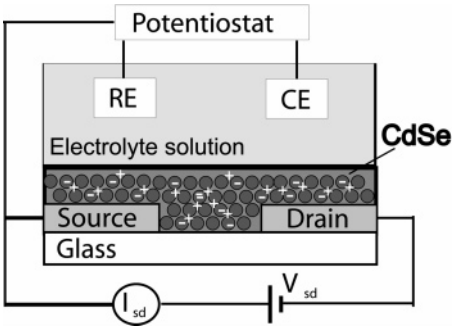

Figure 2. Schematic picture of the electrochemically gated transistor. The sample is submerged in an electrolyte solution. The electrochemical potential of the sample is controlled with respect to a reference electrode (RE) using a potentiostat.

The electrochemical gating setup allows in situ optical and electrical measurements. For optical measurements, the working electrode consisted of a quantum-dot assembly deposited on an ITO substrate. Absorption spectra were obtained with a Perkin-Elmer Lambda 16 UV−vis spectrophotometer. For conductance measurements, a gold source-drain geometry was used (see Figure 2), which allows measurement of the electronic conduction through the film. The width of the gap was 2 μm, and the length was 2 cm.

The conductance in these samples was too low to measure accurately with a small dc bias, so a low-frequency ac bias was applied. The potentials of both source and drain were controlled with a Princeton Applied Research 366A bi-potentiostat. A Krohn-Lite 5200 function generator was used to apply a small ac modulation to the source electrode while the potential of the drain was kept constant. The current was measured with the bi-potentiostat and read out on a Tektronix TDS 420 digitizing

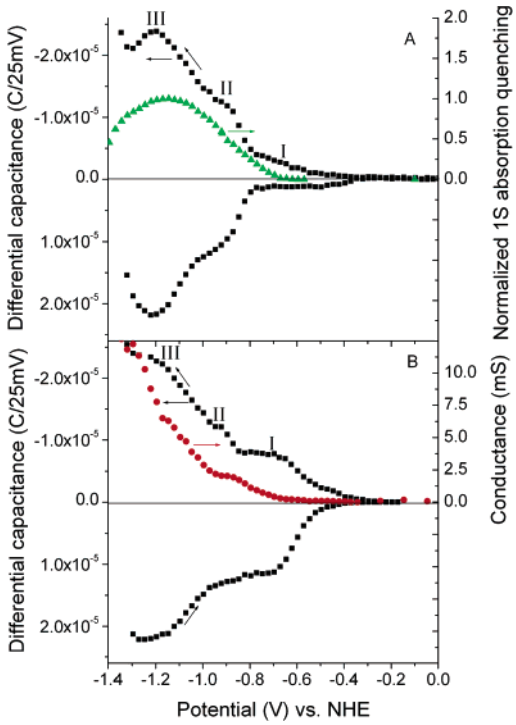

Figure 3. Differential capacitance (black squares in A and B, two different samples) of 6.4 nm CdSe quantum-dot assemblies. Also shown are the normalized absorption quenching (green triangles in A) as a measure of the 1S orbital occupation (see below) and the long-range electronic conduction (red circles in B). The Roman numbers indicate the different features in the charging characteristics. The first wave of electron injection (feature I) clearly occurs before the onset of both the 1S absorption quenching and the electronic conduction; its magnitude is strongly sample-dependent.

oscilloscope. A low frequency (8 Hz) was used to ensure that the ac signal was much slower than the response time of the quantum-dot solid. The conductance was not frequency-dependent at these low frequencies. The source-drain current was always linear with applied bias. This Ohmic behavior ensures that the measurements were done under near-steady-state conditions. At more negative electrode potentials, that is, with increasing electron concentration, the conductance could also be measured with a dc bias and was found to be identical to the conductance determined in the ac mode.

We checked the (electro)chemical stability of the CdSe assembly under conditions of electron charging by incremental steps of the electrochemical potential of the assembly in forward and reverse directions. All measurements reported below were performed under steady-state conditions.

Results and Discussion

Differential Capacitance and Electronic Conductance versus Electrochemical Potential. Electron storage in CdSe quantum-dot solids was first examined by differential capacitance measurements. Results are shown in Figure 3A for 6.4 nm CdSe quantum dots on an ITO substrate. The scale (Coulomb per 25 mV) corresponds to the charge injected in a single potential step of 25 mV. Upon making the electrode potential more negative, electrons are injected into the quantum-dot solid or stored at the ITO/electrolyte interface. To obtain the differential capacitance of the quantum-dot solid, a measurement was also performed on an identical, bare ITO substrate and this (constant) background was subtracted. The resulting differential capacitance clearly shows three waves; note that the forward and the reverse scans are almost identical. This illustrates the quantitative determination of charges injected into—and extracted from—the quantum-dot assembly. Electron injection starts at around −0.45 V versus NHE *independent* of the size of the CdSe nanocrystals in the assembly (feature I in Figure 3). At more negative potentials, a second (II) and a third (III) wave are observed. The onset of these waves occurs at more negative potentials as the size of the CdSe nanocrystals is decreased.

The shape and relative amplitude of the second and third waves are reasonably reproducible from sample to sample. The amplitude of the first wave, however, can show significant differences for different samples. In addition, the onset of the second and third waves is subject to some variation, in some cases up to 300 mV. We remark that a variation in the potential of the reference electrode cannot explain these differences; the reference was always carefully calibrated before and after each measurement. Significant differences in the charging potentials were also observed by Yu et al.[21] We show below that the variable onset of electron injection into the conduction orbitals can be understood as a result of Coulomb repulsion of the injected electrons with electrons occupying localized states in the band gap.

The absorption quenching of the $1S_{3/2}1S_e$ transition is also shown in Figure 3A. This is a direct measure of the $1S_e$ orbital occupation (see below). It is clear that the electrons injected in the first wave do not lead to quenching of this transition and, therefore, do not occupy the $1S_e$ conduction orbitals. The observed maximum in the absorption quenching at a potential of −1.2 V, followed by a decrease, is caused by strong optical scattering that is typically observed at potentials more negative than ∼−1.0 V versus NHE (see below). Figure 3B shows the differential capacitance together with the room-temperature conductance of a second sample of 6.4 nm CdSe nanocrystals. The conductance does not increase with the first wave in the differential capacitance, but with the second. Furthermore, there is a second rise in the conductance that appears together with the third wave in the differential capacitance curve.

From both the conductance in Figure 3B and the 1S absorption quenching in Figure 3A, it is evident that electrons are injected into the assembly which do not occupy conduction orbitals. We conjecture that the first wave in the differential capacitance is due to electron injection into localized states, in the band gap of the nanocrystals. These states are very likely related to the nanocrystal surface. The present results differ from those obtained with assemblies of ZnO quantum dots, where the onset of electron injection occurs together with that of electronic conduction and 1S absorption quenching, showing that electron occupation of localized band gap states is not important in that material.[13,27]

To investigate the nature of the localized states and to assign electrons injected at more negative electrode potentials, in situ optical measurements were performed.

Absorption of Charged Nanocrystal Assemblies. The visible absorption spectrum of CdSe quantum dots is characterized by sharp features that originate from different excitonic transitions. The absorption spectrum of a CdSe quantum-dot assembly retains these features. An absorption spectrum of an assembly of 6.4 nm CdSe quantum dots is shown in Figure 4A. The second derivative of this spectrum (Figure 4B) indicates the different optical transition energies that can be assigned on the basis of work by Norris and Bawendi.[17] Also shown in Figure 4 is the second derivative of the absorption spectrum of a dispersion of the same batch of nanocrystals. It is clear that the spectra of the dispersion and the assembly are virtually

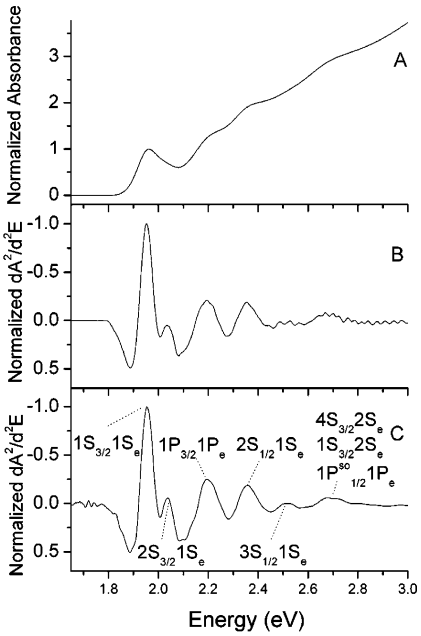

Figure 4. (A) Absorption spectrum of an assembly consisting of 6.4 nm CdSe quantum dots. In this spectrum, several different features can be resolved. (B) Normalized second derivative of A. Negative peaks in the second derivative indicate the different optical transition energies.[28,29] Also shown is the second derivative of an absorption spectrum of a dispersion of nanocrystals of the same size (C). The transitions are assigned according to Norris and Bawendi.[17] It is clear that the absorption spectra of assemblies and dispersions are identical, indicating weak electronic coupling between nanoparticles in these CdSe nanocrystal assemblies.

identical. Electronic coupling between the nanocrystals in the assembly is, thus, weak. The four lowest energy transitions that can be observed in the absorption spectrum are the $1S_{3/2}1S_e$, $2S_{3/2}1S_e$, $1P_{3/2}1P_e$, and $2S_{1/2}1S_e$ excitons. These transitions are indicated in Figure 4C. When the electrode potential is made more negative, electrons are injected into the assembly. The added negative charges can lead to quenching of transitions in the absorption spectrum and to red-shifts of transition energies.

Such a red-shift is caused by the Coulomb interaction of the added electrons (also called spectator charges) with the exciton electron and hole. The spectator electrons can either occupy conduction orbitals or localized states. The positive and negative Coulomb interactions with the exciton hole and exciton electron, respectively, do not completely cancel each other; since the hole orbitals are more localized than the electron orbitals, the attractive Coulomb energy between the spectator electrons and the exciton hole is larger than the repulsive Coulomb energy between the spectator electrons and the exciton electron (see also Figure 5A).[18] This leads to an effective red-shift of all optical transition energies.

Quenching of optical transitions occurs when the injected electrons occupy conduction orbitals in the nanocrystals. These electrons then block transitions involving this conduction level. The case when two electrons occupy the $1S_e$ conduction level is depicted in Figure 5B. There is now no possibility to create an exciton with the electron in the $1S_e$ level: the three transitions involving this $1S_e$ level are quenched. This effect has been coined Pauli-blocking and has been observed for many different semiconductor nanocrystals.[13,14,30−32]

The changes that occur in the absorption spectrum of an assembly consisting of 8.4 nm CdSe quantum dots upon making the electrode potential more negative are shown in Figure 6. In Figure 6A, the different optical transitions of the uncharged

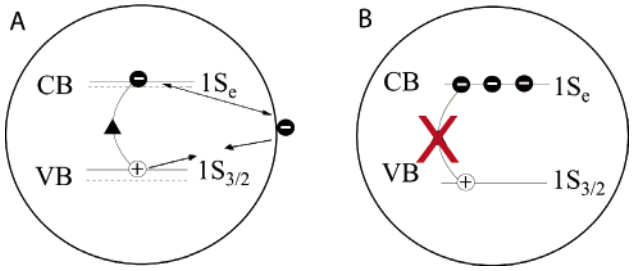

Figure 5. (A) Scheme of Coulomb interactions between a negative spectator charge on the surface of a quantum dot and the exciton electron and hole. The dotted lines are the single-particle energy levels (neutral quantum dot). Since, in CdSe, the hole is more localized than the electron, the net effect of the Coulomb interactions will be a red-shift in the exciton transition energy.[18] (B) Scheme of Pauli blocking due to electron occupation of the $1S_e$ conduction level. If two electrons occupy this level, all transitions involving the $1S_e$ conduction state will be quenched.

assembly are indicated by the second derivative of the absorption spectrum. Figure 6B−E show the absorption difference at different electrode potentials, with respect to the uncharged assembly. At a potential of −0.46 V, one feature can be resolved: a clear oscillation between 1.8 and 2.0 eV, due to a red-shift of the $1S_{3/2}1S_e$ transition energy.[33] The amplitude of this oscillation is small, roughly 100 times smaller than the maximum amplitude of the quenching feature at more negative electrode potentials (see below).

Red-shifts in optical transitions have been observed before,[12,30] but only at more negative electrode potentials, where they were always found together with strong quenching of optical transitions; they were, therefore, attributed to Coulomb interactions between the exciton and electrons in conduction band states. Furthermore, all previously reported red-shifts were only visible as an induced absorption; that is, there was only a maximum and no minimum in the difference spectrum. This was probably caused by overlap of the minimum with quenching features that were the dominant signal in those measurements. In Figure 6B, there is a clear red-shift without any sign of absorption quenching, indicating that there are no electrons occupying conduction orbitals. The observed red-shift, therefore, provides additional evidence that electrons can be injected into the assembly before the $1S_e$ energy level becomes occupied. Since there are no electrons in the conduction orbitals, the red-shift of the $1S_{3/2}1S_e$ excitonic transition could well be explained by the presence of spectator electrons in localized states.

The amplitude of the observed oscillation is 1% of the absorption, and the peak-to-peak separation is ∼0.1 eV. If there is one localized charge per quantum dot, this would correspond to a red-shift in the transition energy of 1 meV per spectator electron. However, the number of localized charges is usually much smaller. This means that the red-shift per surface charge is probably larger than 1 meV. We note that theory predicts shifts in the 10 meV range per spectator charge.[18]

When the electrode potential is made more negative, quenching of excitonic transitions occurs. Figure 6C shows the absorption difference at −0.76 V versus NHE with two clear quenching features at the position of the $1S_{3/2}1S_e$ and $2S_{1/2}1S_e$ transitions indicating (partial) occupation of the $1S_e$ levels. The maximum of the quenching features is red-shifted with respect to the optical transition maxima shown in Figure 6A, since, at this potential, not all nanocrystals are occupied by two electrons, and the electrons will preferentially occupy the larger nanocrystals in the assembly. Only when the $1S_{3/2}1S_e$ and $2S_{1/2}1S_e$

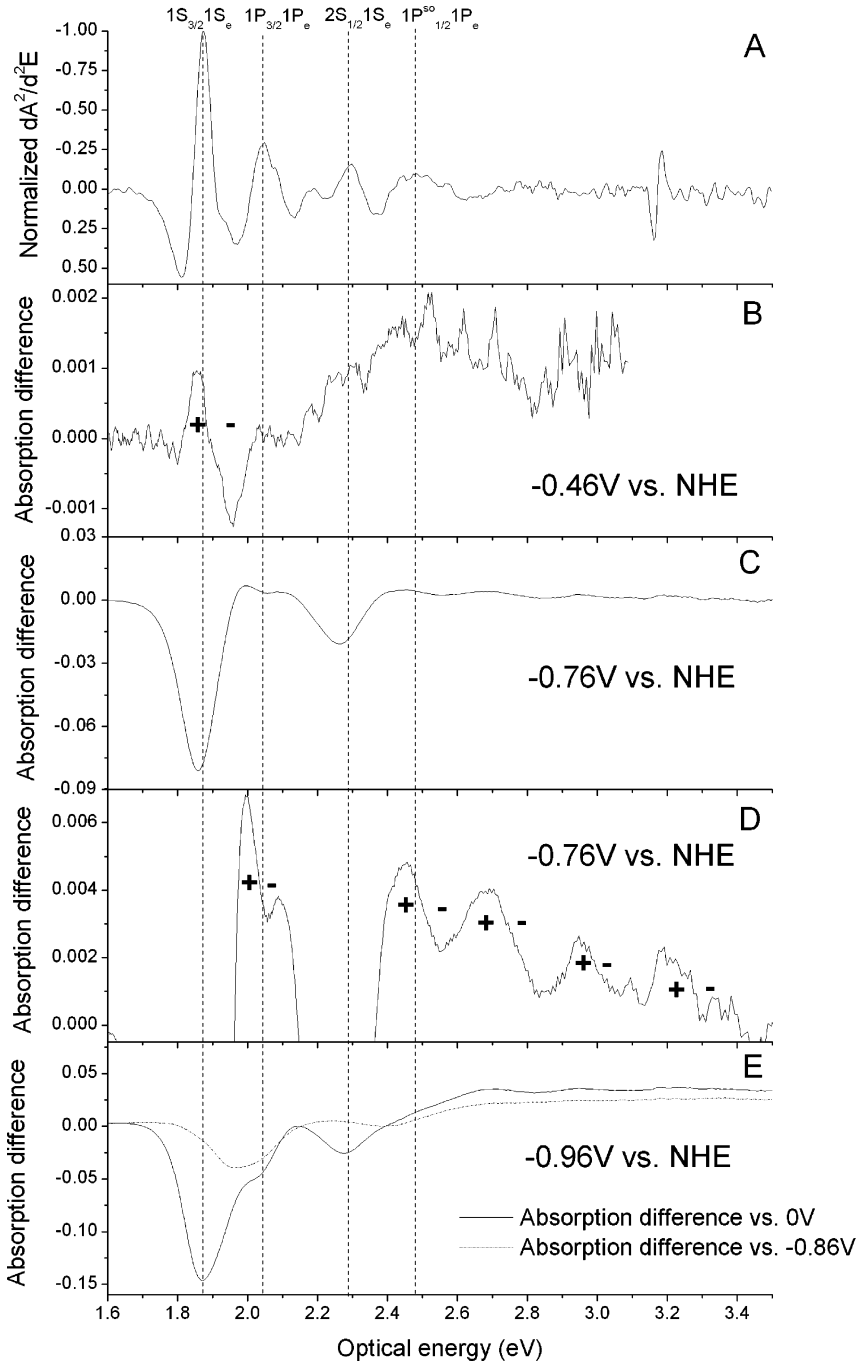

Figure 6. (A) Second derivative for an absorption spectrum of an assembly of 8.4 nm CdSe quantum dots. The four best resolved transitions are indicated. (B) Absorption difference spectrum of the same quantum-dot assembly at −0.46 V vs NHE, before the onset of conductance. No quenching features are observed, only a red-shift of the lowest energy transition. This red-shift is a result of Coulomb interactions with localized spectator electrons. (C) Absorption difference at moderate electrode potential (−0.76 V vs NHE). The two dominant features are the quenching of the $1S_{3/2}1S_e$ and $2S_{3/2}1S_e$ transitions. Also shown is a magnification of part of the same spectrum (D), showing red-shifts of the $1P_{3/2}1P_e$ and higher energy transitions. (E) The absorption difference at −0.96 V vs NHE with respect to the 0 V uncharged state (solid line) and with respect to −0.86 V vs NHE (dashed line). The $1S_e$ transitions are fully quenched, and new features appear, corresponding to quenching of the $1P_{3/2}1P_e$ and $1P^{so}{}_{1/2}1P_e$ transitions (see text).

transitions are fully quenched do the maxima of the quenching features correspond to the uncharged transition maxima (see Figure 6E).

A zoom-in on the absorption difference at −0.76 V versus NHE is shown in Figure 6D and reveals five oscillations that correspond to red-shifts of the $1P_{3/2}1P_e$, $1P^{so}{}_{1/2}1P_e$ (see below for an assignment of this level), and higher energy transitions. Here, these red-shifts are mainly caused by spectator electrons in the $1S_e$ level. Such a multitude of red-shifts in the optical transitions has not been observed before. It illustrates that all excitonic transitions are affected by the additional charges in a similar manner.

At an electrode potential of −0.96 V versus NHE, two additional quenching peaks are found (dashed line in Figure 6E). We believe that these peaks correspond to Pauli-blocking of the $1P_{3/2}1P_e$ and the $1P^{so}{}_{1/2}1P_e$ transitions. The energy of the larger of these features corresponds to the energy of the $1P_{3/2}1P_e$ transition for this size of quantum dots, as determined by Norris and Bawendi.[17] Since the potential dependence of these two quenching features is the same, the smaller feature must also

involve the $1P_e$ level. Norris and Bawendi assigned this absorption peak to the $4S_{3/2}2S_e$, $1S_{1/2}2S_e$, and $1P^{so}{}_{1/2}1P_e$ transitions. The electrochemical gating technique provides evidence that this absorption feature is, at least partly, due to the $1P^{so}{}_{1/2}1P_e$ transition. This is in agreement with a previous assignment by Guyot-Sionnest and Wang.[4]

A comparison of Figures 3 and 6 makes it possible to assign the different waves in the capacitance function: the first wave (I) is caused by electron injection into localized states, the second wave (II) reflects the occupation of the $1S_e$ conduction level with, in total, two electrons, while the third wave (III) is due to the charging of the $1P_e$ conduction level.

The Energetics of Electron Charging: Measurement of the Occupation of $1S_e$ Conduction States. The quenching of a given excitonic transition is a direct measure of the electron occupation of the conduction energy level involved in this transition. If all the quantum dots in the assembly have their $1S_e$ state completely filled, the $1S_e$ transitions must be completely quenched. To quantify the orbital occupation, it is thus appropriate to look at the relative quenching (RQ):

$$RQ_{1S}(V) = -\Delta OD_{1S}(V)/OD_{1S}(0V) = (^1/_2)n_{1S}(V) \quad (1)$$

Here n_{1S} is the average number of electrons in the $1S_e$ state per nanocrystal and the proportionality constant of $^1/_2$ comes from the 2-fold degeneracy of this level.

Although the relative quenching should reach 1 for a $1S_e$ orbital occupation of 2, the highest observed relative quenching in practice was ~0.85. There are several reasons for this. First of all, for the smaller nanocrystals, the potential at which the average number of electrons per quantum dot is 2 might be outside the electrochemical stability window. When the samples are held at potentials below −1.4 V versus NHE, changes in optical properties of the assembly are no longer reversible. A second reason is that higher energy transitions overlap with the $1S_{3/2}1S_e$ transition, leading to a nonzero absorption at this energy even when the $1S_{3/2}1S_e$ transition is fully quenched. Finally, we have observed a strong scattering with a λ^{-4} dependence, when the potential of the assemblies is made more negative. This scattering is the main reason the observed relative quenching maximum is smaller than 1. After a certain potential, the relative quenching even seems to decrease. This is a result of the fact that the optical scattering strongly increases as the potential is made more negative. The extinction increases as a result of this scattering, which leads to a smaller value of the measured 1S quenching.

The exact origin of the increased scattering is unknown and was not systematically investigated. However, it does not depend on the type of substrate or on the thickness of the assembly but only on the electrode potential. Upon changing the electrode potential back to 0 V, the scattering disappears completely.

To correct for variations in the relative quenching, the curves have been normalized. This is justified by the fact that, often, the quenching of $1P_e$ transitions still increased after the $1S_e$ quenching was saturated, suggesting that the $1S_e$ level is, indeed, fully occupied. Normalizing the relative quenching leads to the curves shown in Figure 7A, where the occupation of the $1S_e$ level is plotted for different sizes of quantum dots. They are obtained by monitoring the quenching of the $1S_{3/2}1S_e$ transition. The quenching of, for example, the $2S_{1/2}1S_e$ transition gives essentially the same curves, although the maximum observed relative quenching is smaller. Here, the potential dependence of the quenching is quantified by the potential at with the number of $1S_e$ electrons per quantum dot is 1: the "quenching potential".

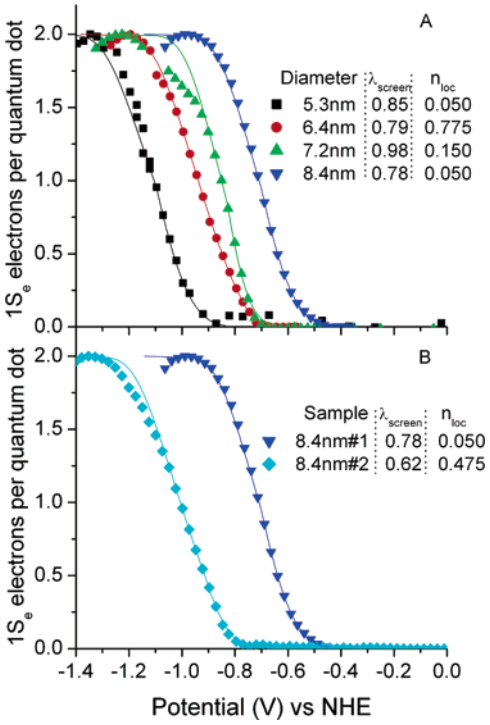

Figure 7. Electron occupation of the $1S_e$ level per quantum dot in an assembly of CdSe nanocrystals. The symbols are experimental data points; the solid lines are fits obtained with the model outlined in the text. The upper graph (A) is an overview of four different sizes of nanocrystals showing that, in general, smaller quantum dots show quenching at more negative potentials. The lower graph (B) shows a comparison of two samples of 8.4 nm CdSe quantum dots, exhibiting a strong variation in the quenching potential (see text).

As was previously shown by Wang et al.,[14] it is more difficult to charge smaller quantum dots. For small quantum dots, the quenching potential is more negative than for large quantum dots. Although there is a clear trend in the results of Figure 7A, the exact quenching potential is not completely reproducible. Figure 7B shows a comparison of two samples with quantum dots of the same size, showing a strong difference in quenching potential. The same difference can be observed in the corresponding differential capacitance scans (not shown); there is a difference of ~0.3 V in the onset of the second wave of electron injection.

We conjecture that such anomalies are due to the effect of electrons trapped in band gap states, probably at the surface of the quantum dots; negative charges lead to a shift of the electrochemical potential for electron addition in the $1S_e$ level. Different samples may have a different average number of such electron states. This will be discussed below.

In Figure 8, the quenching potentials of assemblies consisting of CdSe quantum dots with diameters ranging from 5 to 9 nm are plotted as a function of the single particle confinement energies.[34] The line is a guide to the eye. If the electrochemical potential of electron addition (i.e., the quenching potential) was only determined by the single-particle addition energy of the nanocrystals, the slope of the line in Figure 8 should be close to −1. In practice, it is almost −3, indicating that, besides the quantum-confinement energy, there are other important factors determining the electron-addition energy for the $1S_e$ level in assemblies. The strong dependence of the electrochemical potential of electron injection on the confinement energy must be caused by Coulomb repulsions.

The broadening of the electrochemical potential for electron addition to the $1S_e$ level (see Figure 7) can be due to several

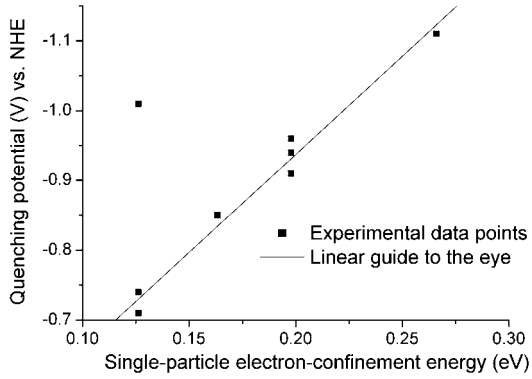

Figure 8. Quenching potential of CdSe quantum-dot assemblies of different nanocrystal sizes, as a function of the single-particle electron-confinement energy. The line is a guide to the eye that illustrates the strong dependence of the quenching potential on the confinement energy: the slope of this line is ~ -3. This is an indication that, besides confinement energy, there are other important factors that determine the electrochemical potential of electron addition.

effects: (i) the homogeneous line width of the $1S_e$ level, (ii) the size dispersion in the ensemble of nanocrystals, and (iii) Coulomb interactions with charges present in the assembly. For the distribution of the $1S_e$ energy level in the assembly (effects i and ii), we have taken a Gaussian function. This is motivated by the observation that both the absorption and the emission corresponding to the first exciton ($1S_{3/2}1S_e$) is accurately described by a Gaussian function of energy.

If Coulomb interactions can be neglected, the relation between the number of $1S_e$ electrons per quantum dot and the electrochemical potential (μ_e) is given by

$$n_{1S}(\tilde{\mu}_e) = \frac{1}{w\sqrt{2\pi}} \int_{-\infty}^{\infty} \frac{e^{-(E-E_{1S})2/2w^2}}{1 + e^{(E-\tilde{\mu}_e)/kT}} dE \qquad (1)$$

where E_{1S} is the center of the broadened $1S_e$ energy level.

The Gaussian width w in eq 1 can be estimated from the absorption spectrum of a dispersion of quantum dots. In these spectra, the first transition peak is well-resolved. The width of this absorption feature is determined by the homogeneous widths of the $1S_e$ conduction level and the $1S_{3/2}$ valence level and by the inhomogeneous broadening due to size dispersion. The inhomogeneous broadening is the main cause of broadening. Since the effective mass of holes in CdSe is significantly larger than the effective mass of electrons, the inhomogeneous broadening of the hole level will be smaller. The Gaussian width of the optical transition can, therefore, be used as an *upper* estimate for the (Gaussian) inhomogeneous width of the $1S_e$ level.

Figure 9 shows the $1S_e$ electron occupation for an assembly consisting of 8.4 nm CdSe quantum dots. The Gaussian width of a dispersion of the quantum dots shown in Figure 9 is 56 meV. The black curve is obtained by entering this value as the Gaussian width w in eq 1. Clearly, the real charging curve has a different shape and is more broadened than the calculated curve. It is, thus, evident that there are more causes of broadening than the homogeneous line width and the polydispersity of the ensemble of quantum dots. It has been noted previously that the dependence of charging on potential can be fitted accurately with an effective temperature of 620 K, but no satisfactory explanation has been put forward.[4] It has also been suggested that the additional broadening may be caused by the charging energy of the nanocrystals, since the $1S_e$ state can accommodate two electrons.[4] However, since the broadening

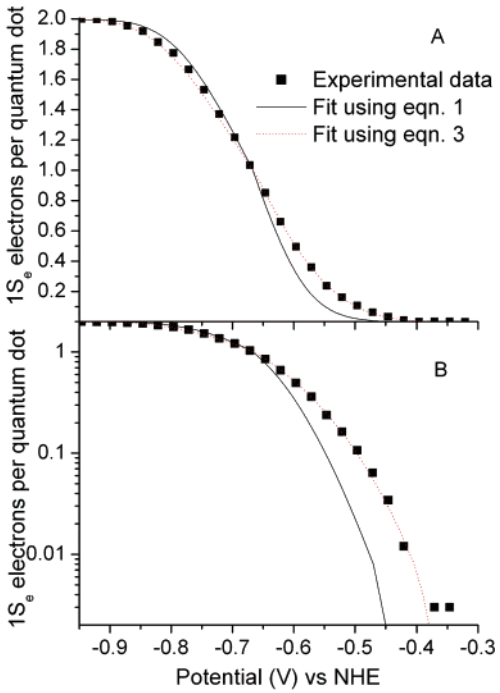

Figure 9. $1S_e$ orbital occupation as a function of potential for an assembly of 8.4 nm quantum dots shown on a linear scale (A) and a logarithmic scale (B). The symbols are experimental data points; the black, solid line is a calculated curve based on the inhomogeneous broadening of the $1S_e$ level. The dotted, red curve is obtained with a model that includes electron repulsion within the assembly (see text).

is also apparent at low electron occupation where there is less than one electron per quantum dot, the intraparticle electron−electron repulsion (i.e., the charging energy) alone cannot explain the extra broadening. Below, we propose a simple model that takes into account the Coulomb repulsion of the injected electron with *all* electrons that are present in the assembly, not only the electrons present within one given quantum dot.

The Energetics of Electron Charging: A Model Based On Electronic Coulomb Repulsion in and between the Nanocrystals. In the electrochemical charging of thin films, it has usually been assumed that counterions from the electrolyte permeate the whole film and effectively screen all nanoparticles from their surroundings.[10,13,24,25,35] We propose here that the electrolyte screening is effective but not complete. If this is so, the Coulomb repulsion between electrons on neighboring quantum dots will not be negligible. The electrons may reside in conduction band energy levels or in localized states. For simplicity, we make no distinction between these cases and assume that their Coulomb potential is the same. We assume an equilibrium situation, where the electrostatic repulsion in the film is minimized. This means the electrons will be distributed such that their mutual separation is maximal, that is, in a face-centered cubic arrangement. A further simplification is that we take into account only the electron repulsion between nearest neighbors.[36] Screening by the electrolyte is taken into account by an adjustable screening parameter λ_{screen}. Calculating the interaction between next-nearest neighbors and electrons at even larger distances can be done but will only lead to a larger screening parameter, not affecting the physical results of this model. When the number of electrons per nanocrystal is larger than 1, there is an additional repulsion energy between electrons within the nanocrystal. This intraparticle repulsion has been calculated for CdSe nanocrystals by Lannoo et al.[34] and is expressed by

$$J_{ee} = \left(\frac{1}{\epsilon_{out}} + \frac{0.79}{\epsilon_{in}}\right)\frac{e}{2\pi\epsilon_0 d_{nc}} \quad (2)$$

Here d_{nc} is the nanocrystal diameter, ϵ_{in} is the dielectric constant of the CdSe nanocrystals, which is taken to be 8.9,[34,37] and ϵ_{out} is the static dielectric constant outside the nanocrystals. This will be some value determined by the solvent (acetonitrile, $\epsilon = 37.5$), the organic capping layer (pyridine, $\epsilon = 12.5$), and the counterions. We have used the dielectric constant of acetonitrile for the calculations described here, but note that the electron repulsion is very insensitive to this value as long as it is larger than ~10.

The final function describing the number of electrons per quantum dot that reside in a 1Se level now becomes[38]

$$n_{1S}(\tilde{\mu}_e) = \frac{1}{w\sqrt{2\pi}}\int_{-\infty}^{\infty}\frac{e^{-(E-E1_S-E_{rep})2/2w^2}}{1+e^{(E-\mu_e)/kT}}\,dE \quad (3)$$

The total electron repulsion E_{rep} depends on the total number of electrons per nanocrystal $n = n_{1S} + n_{loc}$; n_{loc} is the number of electrons per nanocrystal trapped in band gap states. For $n \leq 1$, the repulsion energy is given by

$$E_{rep}(\tilde{\mu}_e) = (1-\lambda_{screen})\frac{3e^2 n^{1/3}(\tilde{\mu}_e)}{d_{nc}\pi\epsilon\epsilon_0} \qquad n \leq 1 \quad (3b)$$

while for $n > 1$, it becomes

$$E_{rep}(\tilde{\mu}_e) = (1-\lambda_{screen})\frac{3e^2 n^{1/3}(\tilde{\mu}_e)}{d_{nc}\pi\epsilon\epsilon_0} + (n-1)J_{ee} \qquad n > 1 \quad (3c)$$

As n appears on both sides of eq 3, it was solved self-consistently.

In this model, there are two system parameters: the screening factor λ_{screen} and the number of localized states per nanocrystal n_{loc}. These two parameters determine the shape of the charging curves shown in Figures 7 and 9 and also determine the shift of the electron-addition energy with respect to the single-particle-addition energy (see Figure 8). The same unique combination of these parameters invariably leads to the best description of the experimental data.

The red curve in Figure 9 is calculated using eq 3 with a screening factor of 0.78 and 0.05 localized states per quantum dot. Figure 7A shows the occupation of the $1S_e$ orbitals as a function of potential, for different sizes of quantum dots, with their matching fits according to eq 3. Although the Coulomb repulsion is simplified in this crude model, it describes the experimental data very well, especially for low electron occupation. It is clear that electron−electron repulsions, also those between electrons not present in the same nanocrystal, have to be included to explain the charging characteristics of CdSe quantum-dot solids.

The best fits require a variation in the screening parameter λ_{screen} and the number of localized band gap states n_{loc} from sample to sample. λ_{screen} usually varies between 0.7 and 1. It is not yet clear whether this is related to the microscopic structure of the assembly. The variation in the electrochemical potential of electron injection of the CdSe quantum-dot solids can be explained by the variation in the density of localized states in the assemblies. The electron repulsion shifts the electron-addition energy to values higher than one would expect on the basis of the single-particle-addition energy. Indeed, looking at Figure 7B, the larger number of localized states and the smaller screening parameter necessary to describe the shape of the left curve (diamonds) largely explain the more negative quenching potential of this sample. The trend seen in Figures 7 and 8 of steeply increasing electron-addition energy with decreasing nanocrystal size is also qualitatively explained by the described model: the electron repulsion is larger for smaller diameters, shifting the electron-addition energy to higher values.

Conclusions

In summary, we have measured and assigned electrons injected into CdSe quantum-dot assemblies by using a combination of optical and electrochemical techniques. We have shown that this combination can be used to determine localized and delocalized orbital occupation in an unambiguous way. Furthermore, we have shown that charge interactions shift the energy of all excitonic transitions to the red and that this effect is clearly visible in the absorption spectra of quantum-dot systems charged with electrons in both localized and delocalized orbitals.

Finally, we have demonstrated that Coulomb repulsion between nanocrystals cannot be neglected in the charging characteristics. Repulsion leads, in principle, to a uniform spreading of the electrons over the $1S_e$ orbitals in the assembly. Our simple electron repulsion model can explain the observed differences in the electron-addition energy of different samples, the broadening of the electron occupation as a function of potential, and the strong dependence of the electron-addition energy on diameter.

In general, we have shown that the charge located in electron traps plays an important role in the charging characteristics of the assembly, and in shifts of the excitonic transitions. The strong variation in the density of these electron traps that we encountered suggests that they are not intrinsic to the CdSe quantum dots. We believe that the electron traps are related to chemical impurities such as O_2 and H^+ that absorb on the nanocrystal surface in the assembly, for instance, $O_2 + e^- \rightarrow O_2^-$. Although all measurements were performed under inert conditions, a small amount of gaseous impurities could be present. It is clear that such effects must be avoided in future optoelectronic applications based on quantum-dot assemblies.

Acknowledgment. We acknowledge helpful discussions with P. Liljeroth.

Supporting Information Available: A comparison of cyclic voltammetry and differential capacitance and a full mathematical derivation of the model explained in the text. This material is available free of charge via the Internet at http://pubs.acs.org.

References and Notes

(1) Murray, C. B.; Kagan, C. R.; Bawendi, M. G. *Annu. Rev. Mater. Sci.* **2000**, *30*, 545.
(2) Weller, H. *Adv. Mater.* **1993**, *5*, 88.
(3) Alivisatos, A. P. *J. Phys. Chem.* **1996**, *100*, 13226.
(4) Guyot-Sionnest, P.; Wang, C. *J. Phys. Chem. B* **2003**, *107*, 7355.
(5) Germeau, A.; Roest, A. L.; Vanmaekelbergh, D.; Allan, G.; Delerue, C.; Meulenkamp, E. A. *Phys. Rev. Lett.* **2003**, *90*.
(6) Coe, S.; Woo, W. K.; Bawendi, M.; Bulovic, V. *Nature* **2002**, *420*, 800.
(7) Dabbousi, B. O.; Bawendi, M. G.; Onitsuka, O.; Rubner, M. F. *Appl. Phys. Lett.* **1995**, *66*, 1316.
(8) Colvin, V. L.; Schlamp, M. C.; Alivisatos, A. P. *Nature* **1994**, *370*, 354.
(9) Wang, C. J.; Wehrenberg, B. L.; Woo, C. Y.; Guyot-Sionnest, P. *J. Phys. Chem. B* **2004**, *108*, 9027.
(10) Meulenkamp, E. A. *J. Phys. Chem. B* **1999**, *103*, 7831.
(11) Noack, V.; Weller, H.; Eychmuller, A. *J. Phys. Chem. B* **2002**, *106*, 8514.

(12) Yu, D.; Wang, C. J.; Guyot-Sionnest, P. *Science* **2003**, *300*, 1277.
(13) Roest, A. L.; Kelly, J. J.; Vanmaekelbergh, D.; Meulenkamp, E. A. *Phys. Rev. Lett.* **2002**, *89*.
(14) Wang, C. J.; Shim, M.; Guyot-Sionnest, P. *Appl. Phys. Lett.* **2002**, *80*, 4.
(15) Wehrenberg, B. L.; Guyot-Sionnest, P. *J. Am. Chem. Soc.* **2003**, *125* (26), 7806−7807.
(16) Bakkers, E. P. A. M.; Hens, Z.; Zunger, A.; Franceschetti, A.; Kouwenhoven, L. P.; Gurevich, L.; Vanmaekelbergh, D. *Nano Lett.* **2001**, *1*, 551.
(17) Norris, D. J.; Bawendi, M. G. *Phys. Rev. B* **1996**, *53*, 16338.
(18) Franceschetti, A.; Zunger, A. *Phys. Rev. B* **2000**, *62*, R16287.
(19) Murray, C. B.; Norris, D. J.; Bawendi, M. G. *J. Am. Chem. Soc.* **1993**, *115*, 8706.
(20) de Mello Donega, C.; Hickey, S. G.; Wuister, S. F.; Vanmaekelbergh, D.; Meijerink, A. *J. Phys. Chem. B* **2003**, *107*, 489.
(21) Yu, D.; Wang, C.; Guyot-Sionnest, P. *Science* **2003**, *300*, 1277.
(22) Leatherdale, C. A.; Woo, W. K.; Mikulec, F. V.; Bawendi, M. G. *J. Phys. Chem. B* **2002**, *106*, 7619.
(23) Jarosz, M. V.; Porter, V. J.; Fisher, B. R.; Kastner, M. A.; Bawendi, M. G. *Phys. Rev. B* **2004**, *70*, 195327.
(24) Roest, A. L.; Houtepen, A. J.; Kelly, J. J.; Vanmaekelbergh, D. *Faraday Discuss.* **2004**, *125*, 55.
(25) Hulea, I. N.; Brom, H. B.; Houtepen, A. J.; Vanmaekelbergh, D.; Kelly, J. J.; Meulenkamp, E. A. *Phys. Rev. Lett.* **2004**, *93*.
(26) Noviandri, I.; Brown, K. N.; Fleming, D. S.; Gulyas, P. T.; Lay, P. A.; Masters, A. F.; Phillips, L. *J. Phys. Chem. B* **1999**, *103*, 6713.
(27) Roest, A. L.; Germeau, A.; Kelly, J. J.; Vanmaekelbergh, D.; Allan, G.; Meulenkamp, E. A. *ChemPhysChem* **2003**, *4*, 959.
(28) Fernee, M. J.; Watt, A.; Warner, J.; Cooper, S.; Heckenberg, N.; Rubinsztein-Dunlop, H. *Nanotechnology* **2003**, *14*, 991.
(29) Ellingson, R. J.; Beard, M. C.; Johnson, J. C.; Yu, P.; Micic, O. I.; Nozik, A. J.; Shabaev, A.; Efros, A. L. *Nano Lett.* **2005**, *5*, 865.
(30) Wang, C. J.; Shim, M.; Guyot-Sionnest, P. *Science* **2001**, *291*, 2390.
(31) Haase, M.; Weller, H.; Henglein, A. *J. Phys. Chem.* **1988**, *92*, 482.
(32) Warburton, R. J.; Durr, C. S.; Karrai, K.; Kotthaus, J. P.; Medeiros-Ribeiro, G.; Petroff, P. M. *Phys. Rev. Lett*. **1997**, *79*, 5282.
(33) Upon inspecting Figure 5B, it can be seen that the maximum and minimum of the red-shift feature are separated by ∼100 meV and that the minimum of this feature (which one could mistakably interpret as the original position of the $1S_{3/2}1S_e$ absorption) is visible at a much higher energy than the maximum of the $1S_{3/2}1S_e$ quenching feature. It should be noted, however, that when a Gaussian function is shifted, the separation in the difference signal is larger than the shift until the original and new Gaussian are "fully separated". For a shift in energy that is much smaller than the Gaussian width, the center of the difference signal is a much more accurate fingerprint of the original maximum than the minimum in the difference spectrum. Since the center of the difference spectrum is blue-shifted with respect to the center of the 1S quenching feature, it appears that the shift in energy is most apparent in the smaller nanocrystals in the distribution. This can be explained by the fact that the effect of a surface charge on a small nanocrystal is larger than that on a big nanocrystal.
(34) Lannoo, M.; Delerue, C.; Allan, G. *Phys. Rev. Lett.* **1995**, *74*, 3415.
(35) Hoyer, P.; Weller, H. *J. Phys. Chem.* **1995**, *99*, 14096.
(36) In this context, a nearest neighbour means the nearest injected electron, not the nearest nanocrystal.
(37) Wang, L.-W.; Zunger, A. *Phys. Rev. B* **1996**, *53*, 9579.
(38) A full derivation of this equation is available in the Supporting Information.